

Article

# Identifying p56<sup>lck</sup> SH2 Domain Inhibitors Using Molecular Docking and In Silico Scaffold Hopping

Priyanka Samanta <sup>1</sup> and Robert J. Doerksen <sup>1,2,\*</sup>

<sup>1</sup> Department of BioMolecular Sciences, School of Pharmacy, University of Mississippi, Oxford, MS 38677-1848, USA; psamanta@go.olemiss.edu

<sup>2</sup> Research Institute of Pharmaceutical Sciences, School of Pharmacy, University of Mississippi, Oxford, MS 38677-1848, USA

\* Correspondence: rjd@olemiss.edu; Tel.: +1-622-915-7052

**Abstract:** Bacterial infections are the second-leading cause of death, globally. The prevalence of antibacterial resistance has kept the demand strong for the development of new and potent drug candidates. It has been demonstrated that Src protein tyrosine kinases (TKs) play an important role in the regulation of inflammatory responses to tissue injury, which can trigger the onset of several severe diseases. We carried out a search for novel Src protein TK inhibitors, commencing from reported highly potent anti-bacterial compounds obtained using the Mannich reaction, using a combination of e-pharmacophore modeling, virtual screening, ensemble docking, and core hopping. The top-scoring compounds from ligand-based virtual screening were modified using protein structure-based design approaches, and their binding to the Src homology-2 domain of p56<sup>lck</sup> TK was predicted using ensemble molecular docking. We have prepared a database of 202 small molecules and have identified six novel top hits that can be subjected to further investigation. We have also performed in silico ADMET property prediction for the hit compounds. This combined computer-aided drug design approach can serve as a starting point for identifying novel TK inhibitors that could be further subjected to in vitro studies and validation of antimicrobial activity.

**Keywords:** e-pharmacophore modeling; virtual screening; ensemble docking; core hopping; ADMET predictions; protein–ligand interactions



**Citation:** Samanta, P.; Doerksen, R.J. Identifying p56<sup>lck</sup> SH2 Domain Inhibitors Using Molecular Docking and In Silico Scaffold Hopping. *Appl. Sci.* **2024**, *14*, 4277. <https://doi.org/10.3390/app14104277>

Academic Editor: Marta Erminia Alberto

Received: 1 April 2024  
Revised: 3 May 2024  
Accepted: 10 May 2024  
Published: 17 May 2024



**Copyright:** © 2024 by the authors. Licensee MDPI, Basel, Switzerland. This article is an open access article distributed under the terms and conditions of the Creative Commons Attribution (CC BY) license (<https://creativecommons.org/licenses/by/4.0/>).

## 1. Introduction

In 2019, according to the findings published in *Lancet* by the Global Research on Antimicrobial Resistance (GRAM) Project, bacterial infections were the second-leading cause of death globally, yielding 7.7 million deaths [1]. Due to the rise in antimicrobial-resistant bacteria, the annual global healthcare cost of bacterial infections has increased dramatically. Some pathogenic bacteria express fibers tipped with adhesins that bind to and penetrate the epithelial cell surface of the host tissues to reach the mucosa, the bloodstream, and finally to several organs, causing severe and chronic inflammation [2]. The invasion of bacteria is dependent upon the activation of protein tyrosine kinases (TKs) [3–5]. Martinez et al. have demonstrated that inhibition of the protein TKs can block this adhesin-mediated uptake into cells [6]. In another study by Esen et al., it was shown that TK inhibitors prevent the uptake of pathogenic bacteria into rabbit corneal epithelial cells [2].

In 2020–2021, several druggable compounds with significant binding affinity towards the Src homology-2 (SH2) domain of p56<sup>lck</sup> TKs were synthesized using the Mannich reaction and tested [7,8]. Src protein TKs have demonstrated an important role in the regulation of inflammatory responses in tissue cells [9–12]. Animal studies have demonstrated that Src protein TK inhibitors can reduce tissue injury and improve the health of patients suffering from several pathological conditions that cause inflammatory responses [9]. SH2 domains

are known to interact with phosphorylated tyrosine residues in proteins and mediate TK signal transduction [13,14]. P56<sup>lck</sup> (LcK) is an Src-like, lymphocyte-specific TK which has an SH2 domain of ~100 amino-acid residues [15]. In this study, we have used a combination of computer modeling techniques to identify novel small molecules that are predicted to bind strongly to the SH2 domain of P56<sup>lck</sup> protein TK and act as inhibitors for the treatment of bacterial infections. Utilizing the molecular features of the previously-reported highly potent compounds, we identified top hit compounds from virtual screening, modified the structures of the hit compounds, and studied their binding affinities to the p56<sup>lck</sup> protein TK. Using ligand-based e-pharmacophore modeling, virtual screening, ensemble docking, core hopping, and in silico pharmacokinetic properties prediction, we obtained hit molecules that showed high structural similarity to the known potent compounds and are expected to exhibit significant antibacterial activity. This molecule inhibitor design study can serve as a starting point for identifying potentially novel Src TK inhibitors that could be further subjected to in vitro studies for investigating their antibacterial activity.

## 2. Methods and Materials

**Database generation:** The ligand studies by Sahoo et al. were used as our training set for ligand-based e-pharmacophore model generation [7]. All ligands studied in Sahoo et al. had molecular weights between 350–400 Da and logP values from 2–2.5. These values were used as cut-off criteria for the molecular weight and logP to obtain molecules from the ZINC15 database, focusing only on “In-stock” available compounds with “Standard” reactivity. Additionally, to enhance our searchable database, we allowed molecules with possible charge of 0 and pH selected from the Reference (ref: pH ~7.4) and Middle (mid: approximate pH range of 6.4 to 8.4) ranges [16–18]. 782K compounds (96 tranches) were obtained [16–18]. These compounds were used to prepare a Phase database [19–21]. The small molecules were subjected to LigPrep preparation using a previously described protocol [22]. Possible ionization states of the small molecules were generated at pH 7.0 ± 2.0. High-energy ionization/tautomer states of the molecules were removed. Duplicate ligands were skipped during database generation. A total of 50 conformers were generated and minimized for each small molecule. ADMET properties of the small molecules were calculated using QikProp during database generation [22,23]. Prefiltering by Lipinski’s rules was performed and LigFilter properties were generated. This database was then used for ligand-based e-pharmacophore virtual screening.

**Ligand-based e-pharmacophore modeling:** All 26 small molecules obtained from Sahoo et al. were aligned using the Ligand Alignment tool in Schrödinger and used as the input ligands for e-pharmacophore model generation. First, the ligand alignment tool in Schrödinger was used to align the small molecules using their common structural elements. Following this, e-pharmacophore modeling was performed using Phase [19–21]. The best alignment and common features pharmacophore method was used. A total of 50 conformers were generated for each ligand during the pharmacophore hypothesis generation. A total of 20 ligand-based e-pharmacophore models were generated. The generated Phase database was screened through the best scored e-pharmacophore model, and the top hit compounds were retained. The ligands showing a match to all the generated e-pharmacophore sites in the pharmacophore model were kept for further studies.

**Ensemble docking:** The protein used in this study is the SH2 domain of p56<sup>lck</sup>, which is expressed in T lymphocytes. The protein p56<sup>lck</sup> is a 56 kDa protein TK of the p60<sup>src</sup> family which has both SH2 and Src homology 3 (SH3) domains [24]. A total of seven protein structures that included PDB IDs 1CWD [25], 1CWE [25], 1LKK [26], 1LKL [26], 1BHH [27], 1LCJ [15], and 1BHF [27] were used for molecular docking studies (Figure 1A). All the seven X-ray crystal structures used in this work are specifically of the Src SH2 domain of p56<sup>lck</sup>. The drawback of protein rigidity in molecular docking is somewhat mitigated by using ensemble docking, since any variability found in the ensemble of structures can be thought of as a way of taking into account the protein’s experimentally validated flexibility.

Schrödinger's virtual screening workflow was used for the ensemble docking-based virtual screening. The workflow methodology is shown in Figure 1B.

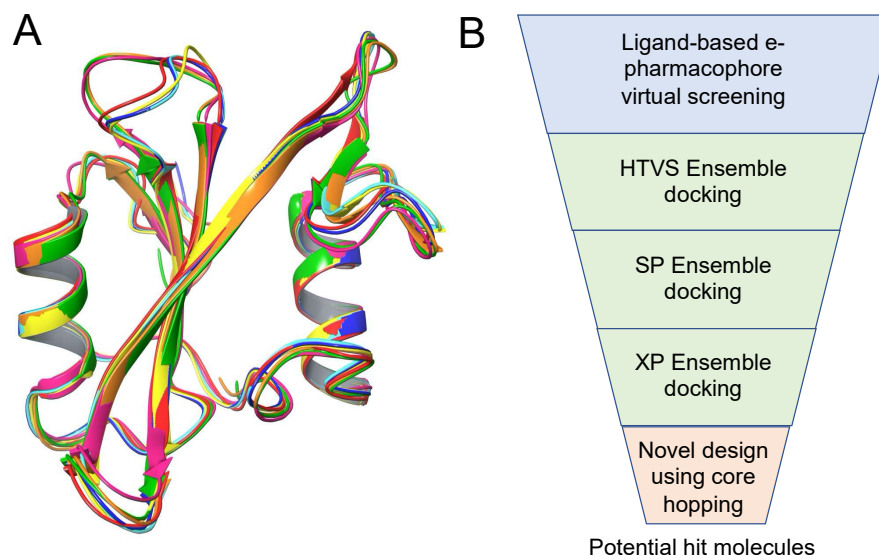


**Figure 1.** (A) Cartoon representation of the 7 protein X-ray crystal structures used for ensemble docking, superimposed on each other (each protein is shown in distinct color). (B) Virtual screening protocol adopted in the study.

**Generation of protein 3D structure:** Water molecules and the co-crystallized ligand molecules were removed from the 7 protein–ligand PDB X-ray crystal structures. The Protein Preparation tool was used, and hydrogens were added to the protein structure using PROPKA at pH 7.0. The OPLS\_2005 force field [28–30] was used to minimize the protein. Two of the PDB structures (PDB ID: 1BHH and 1CWE) are homodimers. In each case, only one chain was retained for these two PDB structures. All protein structures were aligned. Receptor grids were generated for each of the seven protein structures. The centroid of previously identified important binding residues (ResIDs from PDB 1BHF: Arg134, Lys135, Arg154, Glu157, Ser158, Thr159, Ser162, Lys179, His180, Tyr181, Lys182, Ile193, Ser194, Tyr209, Asp214, Gly215, and Leu220) was used as the docking box center [7]. The dimensions of the docking grid size used were  $30 \times 30 \times 30 \text{ \AA}^3$  (inner box) and  $35 \times 35 \times 35 \text{ \AA}^3$  (outer box). First, the ligands shortlisted after screening through the generated e-pharmacophore model were docked using the Glide high-throughput virtual screening (HTVS) protocol. The OPLS\_2005 force field was used for the HTVS docking. The HTVS screened ligands were then subjected to Glide standard precision (SP) docking, followed by Glide extra precision (XP) docking. In the virtual screening protocol, it is standard practice to redock the top 10% of the HTVS scored structures with Glide SP, and then redock the top 10% of SP scored structures with Glide XP [31,32]. Therefore, in our work, 10% of the best docked ligands were retained at each step. The OPLS\_2005 force field was used for the docking runs [33]. During each docking step, the ligands were considered flexible and post-docking minimization was performed.

**Structure-based drug design:** Following the Glide XP ensemble docking, further structural modifications of the top hits were performed to enhance protein–hit interactions, using Core Hopping (CH) in Schrödinger [34]. Starting with the top hit molecule obtained from the multi-step docking workflow, ligand-based and receptor-based CH were performed. CH of the middle scaffold of the reference molecule was performed. To enhance the interactions exhibited in the protein–hit complexes, a minimum cut-off for the number of hydrogen bonds required was set to 5 for the receptor-based CH. Heavy-atom steric clashes with the receptor were limited, with a maximum number of clashing ligand atoms set to 2 and a clash criterion of  $<2.20 \text{ \AA}$ . The Schrödinger CH library (named `core_library_2014.1-86640.sqlite`) was used for the scaffold searching.

### 3. Results and Discussion

**Ligand-based e-pharmacophore models:** A total of 20 ligand-based e-pharmacophore models were generated (Supplementary Table S1). The best e-pharmacophore model had the highest Survival score and was tied for the highest Phase Hypo score. The best ligand-based Phase e-pharmacophore model was a five-point model (DHRRR\_1) containing three aromatic rings (R), one hydrogen bond donor (D), and one hydrophobic group (H) (Figure 2A). It was used for the virtual screening of the generated Phase database.

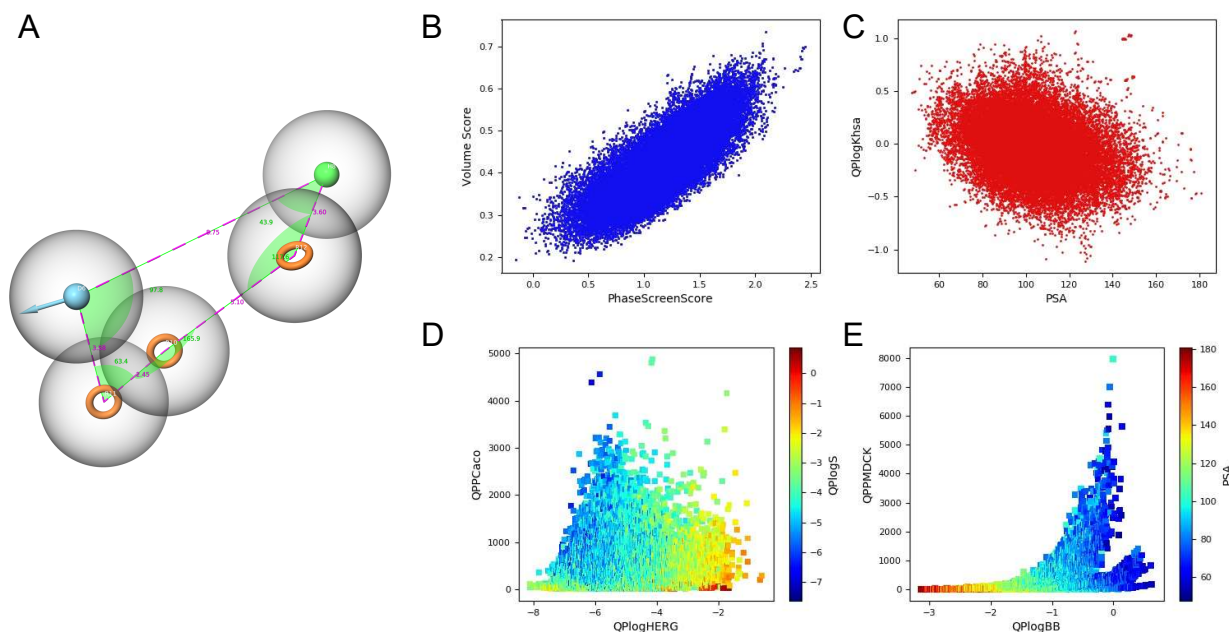


**Figure 2.** Ligand-based e-pharmacophore model and pharmacophore screening scores and predicted physicochemical and pharmacokinetic properties of the successfully screened ligands. (A) Best ligand-based e-pharmacophore model generated. (B) Pharmacophore screening scores. (C–E) Predicted physicochemical and pharmacokinetic properties of the ligands obtained after screening through the best e-pharmacophore model.

**Pharmacophore-based virtual screening of Phase database:** The generated Phase database was screened against the best ligand-based e-pharmacophore model. The top ~35K molecules were retained that matched 5 of 5 e-pharmacophore sites in the ligand-based e-pharmacophore model. The ligand and pharmacokinetic properties of the successfully screened ligands that were retained are shown in Figure 2B–E. The Phase screen scores and the volume scores after e-pharmacophore screening are shown in Figure 2B. The ligands showed predicted binding to human serum albumin within a range of  $-1.0$  to  $+1.0$ , thereby falling within the recommended range of values (Figure 2C). A QPPCaco value (predicted apparent Caco-2 cell permeability in nm/s) of  $>500$  is typically recommended; all ligands showed a value of  $>500$  (Figure 2D). A predicted  $IC_{50}$  of  $<-5$  for the blockage of human ether-a-go-go-related gene (hERG)  $K^+$  channels (QP log<sub>HERG</sub>) is not recommended. Therefore, the ligands that showed a value  $>-5$  could be considered for further drug design purposes (Figure 2D). The predicted apparent Madin–Darby Canine Kidney (MDCK) cell permeability values were  $>500$  nm/s, thus falling within the recommended range (Figure 2E). However, some molecules exhibited a value of  $<500$  nm/s for the MDCK cell permeability as well. Such molecules could be further investigated using alternate permeability prediction models for accurate prediction of their permeability properties. Additionally, the values of the predicted brain/blood partition coefficient also fell within the recommended range ( $-3.0$  to  $1.2$ ) (Figure 2E).

**Ensemble docking-based virtual screening:** Following the steps as mentioned under Section 2, ensemble docking was performed using the top ~35K ligands that were

obtained from e-pharmacophore-based virtual screening. At the end of Glide XP docking, 202 molecules were retained. All 202 molecules showed a negative docking score with XP GScore of  $<-4.278$  kcal/mol. The top hit molecule (Figure 3A) obtained at the end of ensemble docking showed a docking score of  $-6.530$  kcal/mol. The hit compound exhibited four hydrogen bonding interactions with the 1LKL protein (Figure 3B). The ligand binding site is depicted in Figure 3C–D. This hit molecule was then subjected to ligand-based CH and receptor-based CH for novel small molecule design. The top 10 hit molecules from the pool of 202 ligands obtained after virtual screening using ensemble docking are shown in Supplementary Figures S1 and S2. Supplementary Figure S1 shows the 2D structures of the top 10 hit ligands, while Supplementary Figure S2 depicts the docked poses into the ligand binding site on the protein.

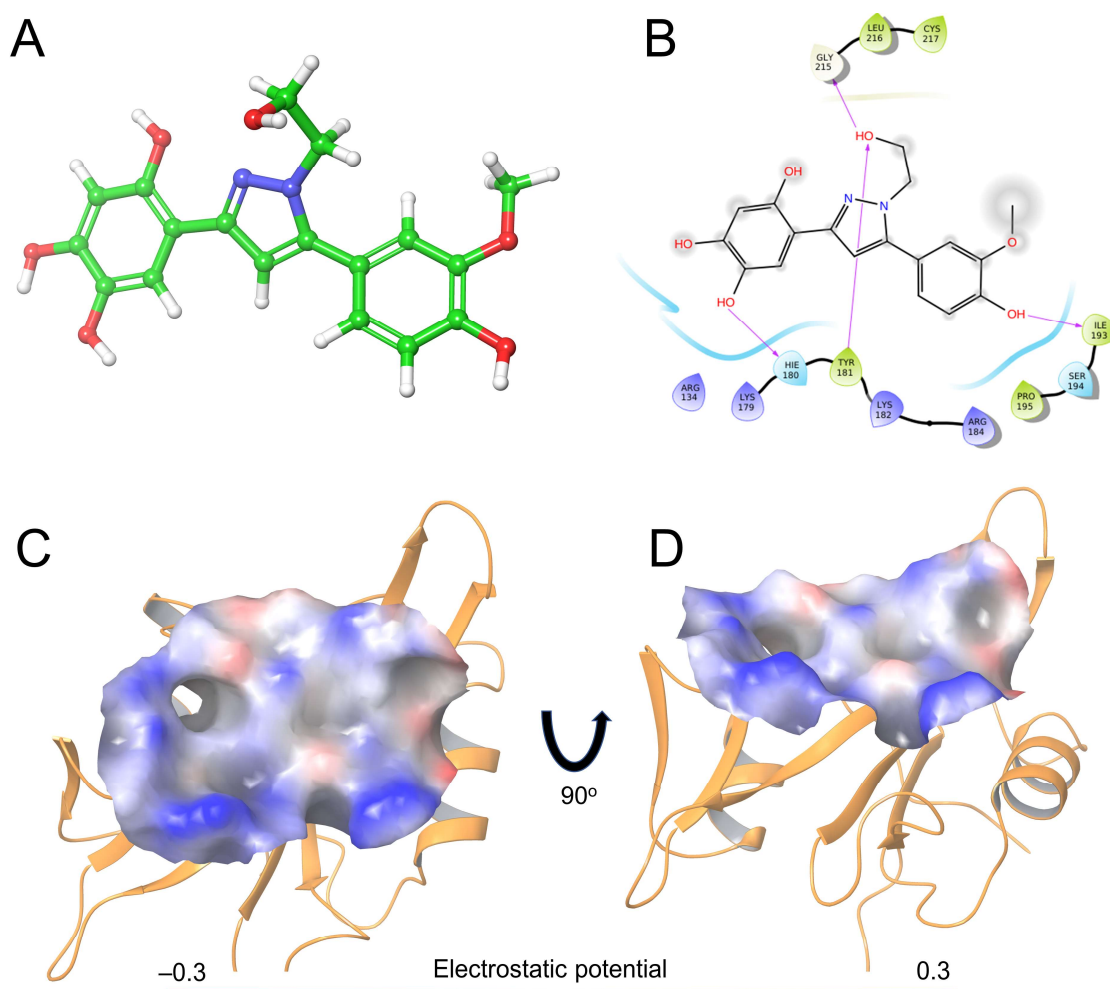


**Figure 3.** Top hit molecule obtained from ensemble docking-based virtual screening (ZINC ID: ZINC000257313939), IUPAC name: 5-(5-(4-hydroxy-3-methoxyphenyl)-1-(2-hydroxyethyl)-1H-pyrazol-3-yl)benzene-1,2,4-triol. (A) 3D structure of the top hit molecule. (B) Interactions between the top hit molecule and the p56<sup>lck</sup> TK protein residues (PDB ID: 1LKL). (C,D) Two viewpoints of the ligand binding site are shown in surface representation. The p56<sup>lck</sup> TK protein (PDB ID: 1LKL) is shown in surface representation and colored using the electrostatic potential (red represents an electrostatic potential value of  $-0.2$  kT/e; blue represents an electrostatic potential value of  $+0.2$  kT/e).

**Ligand-based core hopping (LCH):** The best scored docked hit molecule obtained from ensemble docking-based virtual screening (Figure 3A) was used as the reference in ligand-based core hopping (LCH). Two scaffold growing points were selected on the reference molecule to replace the middle scaffold of the molecule (Figure 4A). A total of 1933 core hopped structures were obtained. Hits obtained from LCH were grouped based

on three categories: overlap score, synthesizability score, and side chain root-mean-square deviation (RMSD) values. The best scored compounds from these three categories were selected as our potential hit compounds. The overall poses of these three hits (1–3) and the reference molecule complexed with the protein surface are shown in Figure 4B. The IUPAC names of the hits 1, 2, and 3 are as follows: 1  $\equiv$  5-((2R,3R,4S,5R)-4-hydroxy-2-(4-hydroxy-3-methoxyphenyl)-2,5-dimethyltetrahydrofuran-3-yl)benzene-1,2,4-triol; 2  $\equiv$  5-(((1R,3R)-1-hydroxy-3-(4-hydroxy-3-methoxyphenoxy)cyclohexyl)methyl)benzene-1,2,4-triol; and 3  $\equiv$  (1S,2R,3R,5S)-2-hydroxy-1-((4-hydroxy-3-methoxyphenoxy)methyl)-2,5-dimethyl-3-(2,4,5-trihydroxyphenyl)cyclopentan-1-aminium.

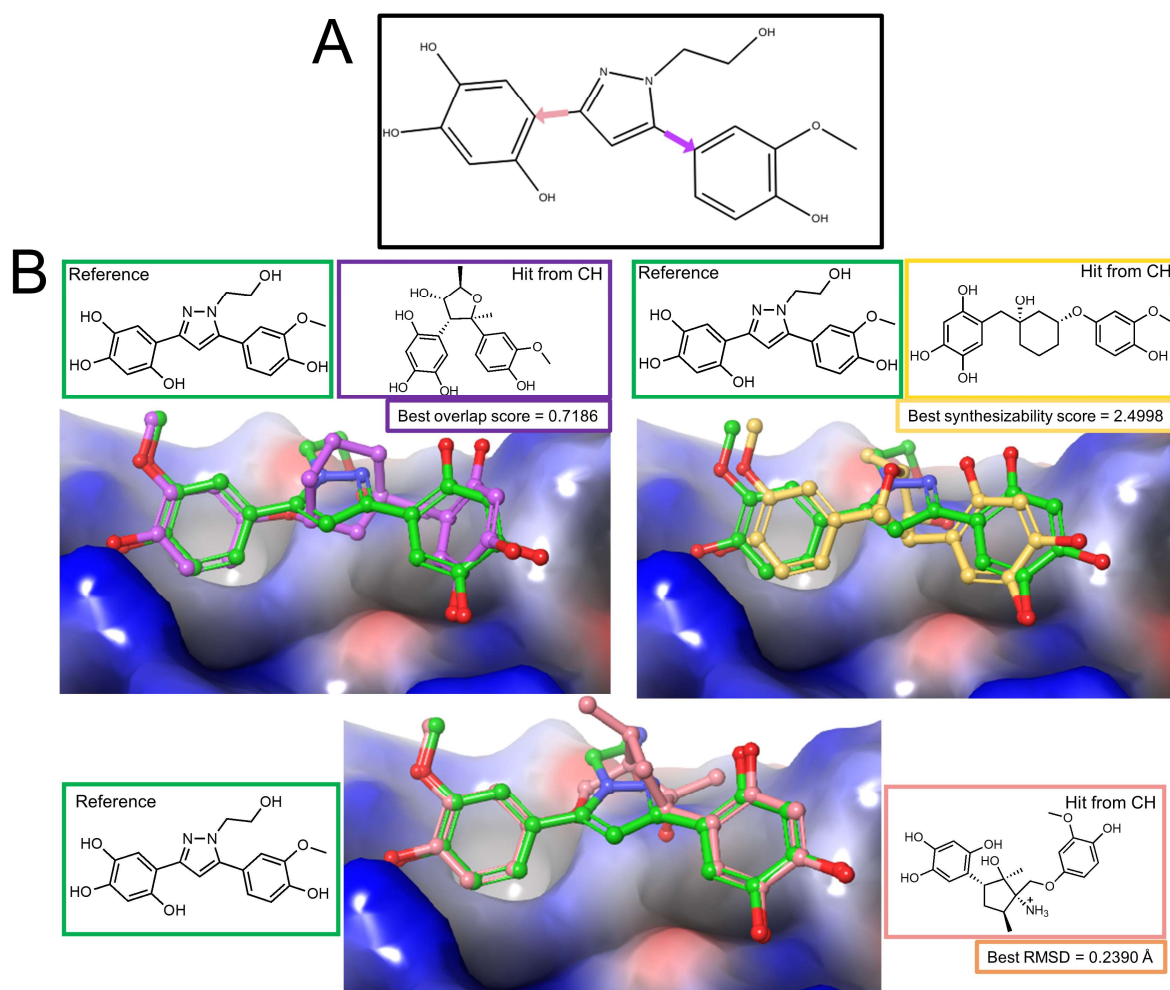


**Figure 4.** (A) Template assignment for scaffold growing in core hopping, CH (core between the pink and purple arrows will undergo hopping). (B) The top three hit compounds (1–3) obtained from ligand-based core hopping (LCH). Green represents the reference molecule (the top hit from ensemble docking-based virtual screening). Purple, yellow, and pink represent the top hit compounds obtained from LCH. The p56<sup>lck</sup> TK protein (PDB ID: 1LKL) is shown in surface representation and colored using the electrostatic potential (red represents an electrostatic potential value of  $-0.2$  kT/e; blue represents an electrostatic potential value of  $+0.2$  kT/e).

**Receptor-based core hopping (RCH):** The best-scored docked hit molecule obtained from ensemble docking-based virtual screening (Figure 3A) was used as the reference in receptor-based core hopping (RCH). This reference hit molecule exhibited four hydrogen bonding interactions with the SH2 domain of p56<sup>lck</sup> TK. To enhance the interactions exhibited in the protein–hit complexes, a minimum cut-off for the number of hydrogen bonds requirement was set to 5. The top two hits (4 and 5) obtained from RCH are shown in Figure 5. We observed that the novel central scaffold obtained after replacement using

the core hopping technique can exhibit a significant number of new hydrogen bonding interactions with the receptor. It should be noted that one of the hits from RCH (shown in cyan; Figure 5 left) showed a synthesizability score of 0, indicating that the ease of synthesis of this molecule is a matter of further investigation. The IUPAC names of the hits 4 and 5 are as follows: 4  $\equiv$  (1R,2R,4R,5R,E)-1-amino-4-hydroxy-2-(4-hydroxy-3-methoxyphenoxy)-5-(2,4,5-trihydroxyphenyl)-6-thiabicyclo[3.2.1]octan-8-one oxime; and 5  $\equiv$  6-(4-hydroxy-3-methoxybenzyl)-2-oxo-N-(2,4,5-trihydroxybenzyl)-2,3-dihydro-1H-thieno[3,4-d]imidazole-1-sulfonamide.

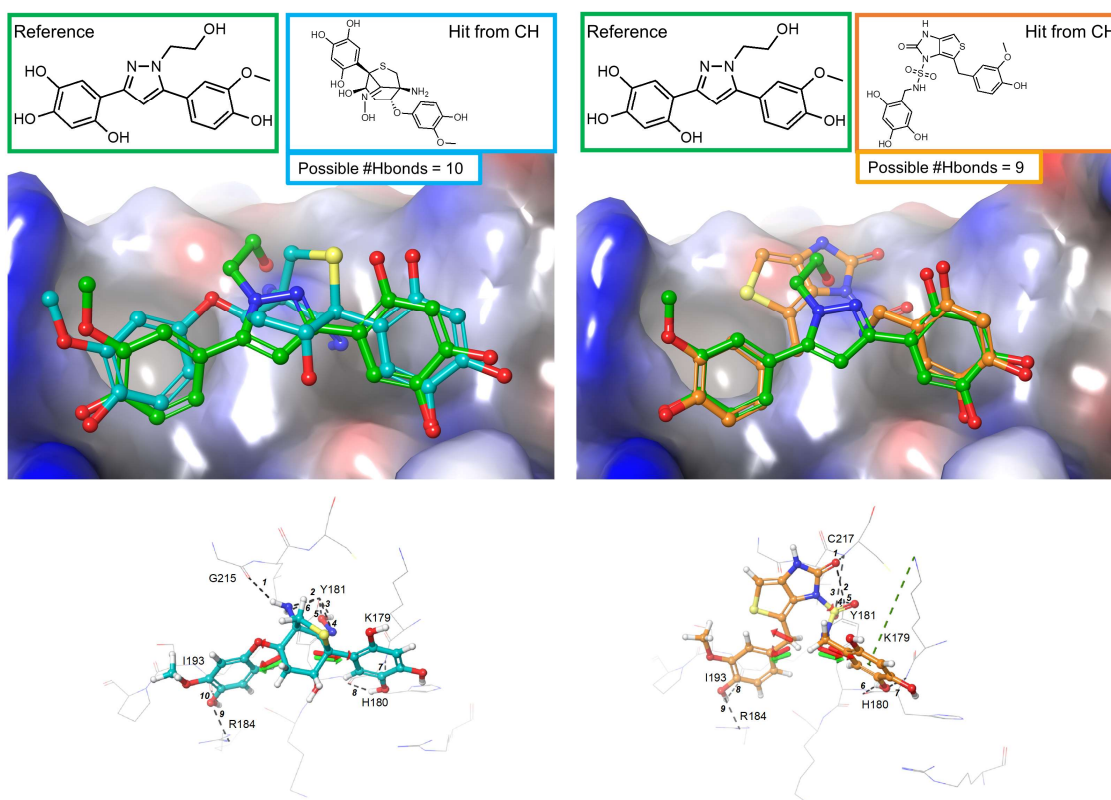


**Figure 5.** The top two hit compounds (4 and 5) obtained from receptor-based core hopping, RCH. Green represents the reference molecule (the top hit from ensemble docking-based virtual screening). Cyan and orange represent the two top hit molecules obtained from RCH. (Top) p56<sup>lck</sup> TK protein (PDB ID: 1LKL) is shown in surface representation and colored using the electrostatic potential (red represents an electrostatic potential value of  $-0.2$  kT/e; blue represents an electrostatic potential value of  $+0.2$  kT/e). (Below) All possible hydrogen bonding interactions with the receptor (dashed lines) that could be exhibited by the hits obtained from RCH [cyan (left) and orange (right)] are shown.

**ADMET prediction of the top hit compounds:** The top five compounds obtained from the ligand-based and structure-based design strategy of CH, along with the reference compound obtained from ensemble-based virtual screening, were subjected to in silico ADMET prediction calculations. The pharmacokinetic properties of the six molecules are summarized in Table 1. The two hits obtained from LCH (1 and 2) showed improved percent oral absorption in the gastrointestinal (GI) and apparent Caco-2 permeability compared to the reference molecule. The model to predict the percent oral absorption is based on a quantitative multiple linear regression, and a value of  $<25\%$  for percent oral absorption is considered poor. The two hits obtained from RCH (4 and 5) exhibited poor percent oral absorption. The predicted apparent MDCK cell permeability (measured in nm/s) is considered to be a good mimic for the blood–brain barrier. A value of QPPMDCK of  $<25$  is considered poor. Two hit compounds from LCH (2 and 3) exhibited poor MDCK cell permeability. 1 from LCH showed slight improvement in MDCK cell permeability

compared to the reference molecule. All compounds fell within the allowed range of QP log  $K_p$  for skin permeability (acceptable range in QikProp is  $-8.0$  to  $-1.0$ ). **3** from LCH and **4** and **5** from RCH showed more negative Log  $K_p$  for skin permeability than the reference molecule and hence are expected to be less skin-permeant.

**Table 1.** Predicted pharmacokinetic properties, calculated using QikProp, of the reference molecule and the five hit molecules (1–5) obtained from ligand-based core hopping (LCH) and receptor-based core hopping (RCH).

Molecule	hERG K <sup>+</sup> (log IC <sub>50</sub> )	% Oral Abs. in the GI	Caco-2 Perm.	MDCK Perm.	QP log K <sub>p</sub> Skin Perm.
Reference	−5.569	64	43	16	−4.559
<b>1</b> (from LCH)	−4.138	72	110	45	−4.254
<b>2</b> (from LCH)	−4.956	70	58	23	−4.279
<b>3</b> (from LCH)	−5.451	42	15	5	−6.353
<b>4</b> (from RCH)	−5.651	18	2	M *	−7.689
<b>5</b> (from RCH)	−5.672	25	5	M *	−5.952

\* M indicates molecular weight is outside the training range. Apparent Caco-2 permeability (Caco-2 perm.) and apparent MDCK permeability (MDCK perm.) are reported in nm/s and QP log  $K_p$  for skin permeability in cm/h.

#### 4. Conclusions

The current study utilized a combination of ligand-based and receptor-based molecular modeling techniques to identify novel small molecules with significant predicted binding to the SH2 domain of p56<sup>lck</sup> tyrosine kinase. Using in silico ADMET prediction approaches, we investigated the pharmacokinetic properties of the five hit small molecules that bound best to the protein of interest. Most of the hits obtained in this study showed high chemical synthesizability, indicating the likelihood that the molecules can be easily synthesized for further in vitro antibacterial studies. Following this study, future investigation using advanced molecular modeling approaches, such as molecular dynamics simulations and binding free energy calculations, can be conducted to obtain a detailed understanding of the protein–hit key pairwise interactions and also to capture the structural dynamics of the hit molecules. It is important to note that the database of 202 small molecules obtained after the e-pharmacophore screening and the results of the ensemble docking can serve as an excellent resource for the discovery of novel inhibitors that can bind strongly to the SH2 domain of p56<sup>lck</sup> TK with significant antibacterial activity. We have also identified six novel hits that can act as an excellent starting point for further investigation.

#### 5. Associated Content

The following file is available free of charge.

The generated e-pharmacophore models and their features; 2D-structures of the top 10 hits from the pool of 202 ligands that were obtained from the virtual screening docking protocol adopted in the study; docked structures of the top 10 hits from the pool of 202 ligands that were obtained from the virtual screening docking protocol adopted in the study.

**Supplementary Materials:** The following supporting information can be downloaded at: <https://www.mdpi.com/article/10.3390/app14104277/s1>, Table S1. The generated e-pharmacophore models and their features. The hypothesis shown in bold is the top ligand-based e-pharmacophore that is used for further studies in this work; Figure S1. 2D-structures of the top 10 hits from the pool of 202 ligands that were obtained from the virtual screening docking protocol adopted in this study; Figure S2. Docked structures of the top 10 hits from the pool of 202 ligands that were obtained from the virtual screening docking protocol adopted in this study. The ligand binding pocket is shown in surface representation. The ligands are shown in gray licorice. The best hit is shown in the first panel in green licorice. SMILES strings and unique ZINC IDs of the 202 molecules are also listed in the supplementary materials.

**Author Contributions:** P.S.: Conceptualization, Methodology, Data Curation, Formal Analysis, Visualization, Investigation, Writing—Original Draft Preparation, Writing—Reviewing and Editing,

Validation. R.J.D.: Conceptualization, Methodology, Writing—Reviewing and Editing, Supervision, Funding Acquisition. All authors have read and agreed to the published version of the manuscript.

**Funding:** This work was supported by the National Institutes of Health [P20GM130460 to R.J.D.]. The content does not necessarily reflect the position or the policy of the sponsors, and no official endorsement should be inferred. The funders had no role in the design or writing, or in the decision to publish the work in this form. The content is solely the responsibility of the authors and does not necessarily represent the official views of the National Institutes of Health.

**Institutional Review Board Statement:** Not applicable.

**Informed Consent Statement:** Not applicable.

**Data Availability Statement:** The data underlying this article are available in the article and in its online Supplementary Material.

**Conflicts of Interest:** The authors declare no conflicts of interest.

## Abbreviations

CH, core hopping; LCH, ligand-based core hopping; RCH, receptor-based core hopping; HTVS, high-throughput virtual screening; SH3, Src homology 3; SH2, Src homology 2; ADMET, adsorption, distribution, metabolism, excretion and toxicity; MD, molecular dynamics; SP, standard precision; XP, extra precision; MDCK, Madin–Darby Canine Kidney; hERG, human ether-a-go-go-related gene; RMSD, root-mean-square deviation; TK, tyrosine kinase.

## References

- Ikuta, K.S.; Swetschinski, L.R.; Aguilar, G.R.; Sharara, F.; Mestrovic, T.; Gray, A.P.; Weaver, N.D.; Wool, E.E.; Han, C.; Hayoon, A.G.; et al. Global mortality associated with 33 bacterial pathogens in 2019: A systematic analysis for the Global Burden of Disease Study 2019. *Lancet* **2022**, *400*, 2221–2248. [[CrossRef](#)]
- Esen, M.; Grassmé, H.; Riethmüller, J.; Riehle, A.; Fassbender, K.; Gulbins, E. Invasion of human epithelial cells by *Pseudomonas aeruginosa* involves src-like tyrosine kinases p60Src and p59Fyn. *Infect. Immun.* **2001**, *69*, 281–287. [[CrossRef](#)]
- Mulvey, M.A. Adhesion and entry of uropathogenic *Escherichia coli*. *Cell Microbiol.* **2002**, *4*, 257–271. [[CrossRef](#)]
- Jorgensen, I.; Seed, P.C. How to make it in the urinary tract: A tutorial by *Escherichia coli*. *PLoS Pathog.* **2012**, *8*, e1002907. [[CrossRef](#)]
- Bergsten, G.; Wullt, B.; Svanborg, C. *Escherichia coli*, fimbriae, bacterial persistence and host response induction in the human urinary tract. *Int. J. Med. Microbiol.* **2005**, *295*, 487–502. [[CrossRef](#)]
- Martinez, J.J.; Hultgren, S.J. Requirement of Rho-family GTPases in the invasion of Type 1-piliated uropathogenic *Escherichia coli*. *Cell Microbiol.* **2002**, *4*, 19–28. [[CrossRef](#)]
- Sahoo, C.R.; Paidesetty, S.K.; Dehury, B.; Padhy, R.N. Molecular dynamics and computational study of Mannich-based coumarin derivatives: Potent tyrosine kinase inhibitor. *J. Biomol. Struct. Dyn.* **2020**, *38*, 5419–5428. [[CrossRef](#)]
- Bishoyi, A.K.; Mahapatra, M.; Paidesetty, S.K.; Padhy, R.N. Design, molecular docking, and antimicrobial assessment of newly synthesized phytochemical thymol Mannich base derivatives. *J. Mol. Struct.* **2021**, *1244*, 130908. [[CrossRef](#)]
- Okutani, D.; Lodyga, M.; Han, B.; Liu, M. Src protein tyrosine kinase family and acute inflammatory responses. *Am. J. Physiol. Lung Cell. Mol. Physiol.* **2006**, *291*, L129–L141. [[CrossRef](#)]
- Armstrong, S.C. Protein kinase activation and myocardial ischemia/reperfusion injury. *Cardiovasc. Res.* **2004**, *61*, 427–436. [[CrossRef](#)]
- Lowell, C.A. Src-family kinases: Rheostats of immune cell signaling. *Mol. Immunol.* **2004**, *41*, 631–643. [[CrossRef](#)]
- Yuan, S.Y. Protein kinase signaling in the modulation of microvascular permeability. *Vascul. Pharmacol.* **2002**, *39*, 213–223. [[CrossRef](#)]
- Ladbury, J.E.; Hensmann, M.; Panayotou, G.; Campbell, I.D. Alternative modes of tyrosyl phosphopeptide binding to a Src family SH2 domain: Implications for regulation of tyrosine kinase activity. *Biochemistry* **1996**, *35*, 11062–11069. [[CrossRef](#)]
- Mulhern, T.D.; Shaw, G.L.; Morton, C.J.; Day, A.J.; Campbell, I.D. The SH2 domain from the tyrosine kinase Fyn in complex with a phosphotyrosyl peptide reveals insights into domain stability and binding specificity. *Structure* **1997**, *5*, 1313–1323. [[CrossRef](#)]
- Eck, M.J.; Shoelson, S.E.; Harrison, S.C. Recognition of a high-affinity phosphotyrosyl peptide by the Src homology-2 domain of p56<sup>lck</sup>. *Nature* **1993**, *362*, 87–91. [[CrossRef](#)]
- Irwin, J.J.; Shoichet, B.K. ZINC—A free database of commercially available compounds for virtual screening. *J. Chem. Inf. Model.* **2005**, *45*, 177–182. [[CrossRef](#)]
- Irwin, J.J.; Sterling, T.; Mysinger, M.M.; Bolstad, E.S.; Coleman, R.G. ZINC: A free tool to discover chemistry for biology. *J. Chem. Inf. Model.* **2012**, *52*, 1757–1768. [[CrossRef](#)]
- Sterling, T.; Irwin, J.J. ZINC 15—Ligand discovery for everyone. *J. Chem. Inf. Model.* **2015**, *55*, 2324–2337. [[CrossRef](#)]

19. Schrödinger Release 2021-2: *Phase*; Schrödinger, LLC: New York, NY, USA, 2021.
20. Dixon, S.L.; Smondyrev, A.M.; Knoll, E.H.; Rao, S.N.; Shaw, D.E.; Friesner, R.A. PHASE: A new engine for pharmacophore perception, 3D QSAR model development, and 3D database screening: 1. Methodology and preliminary results. *J. Comput. Aided Mol. Des.* **2006**, *20*, 647–671. [[CrossRef](#)]
21. Dixon, S.L.; Smondyrev, A.M.; Rao, S.N. PHASE: A novel approach to pharmacophore modeling and 3D database searching. *Chem. Biol. Drug Des.* **2006**, *67*, 370–372. [[CrossRef](#)]
22. Samanta, P.; Doerksen, R.J. Identifying FmlH lectin-binding small molecules for the prevention of *Escherichia coli*-induced urinary tract infections using hybrid fragment-based design and molecular docking. *Comput. Biol. Med.* **2023**, *163*, 107072. [[CrossRef](#)]
23. Schrödinger Release 2021-2: *QikProp*; Schrödinger, LLC: New York, NY, USA, 2021.
24. Amrein, K.E.; Panholzer, B.; Flint, N.A.; Bannwarth, W.; Burn, P. The Src homology 2 domain of the protein-tyrosine kinase p56lck mediates both intermolecular and intramolecular interactions. *Proc. Natl. Acad. Sci. USA* **1993**, *90*, 10285–10289. [[CrossRef](#)]
25. Mikol, V.; Baumann, G.; Keller, T.H.; Manning, U.; Zurini, M.G.M. The crystal structures of the SH2 domain of p56lck complexed with two phosphonopeptides suggest a gated peptide binding site. *J. Mol. Biol.* **1995**, *246*, 344–355. [[CrossRef](#)]
26. Tong, L.; Warren, T.C.; King, J.; Betageri, R.; Rose, J.; Jakes, S. Crystal structures of the human p56lck SH2 domain in complex with two short phosphotyrosyl peptides at 1.0 Å and 1.8 Å resolution. *J. Mol. Biol.* **1996**, *256*, 601–610. [[CrossRef](#)]
27. Tong, L.; Warren, T.C.; Lukas, S.; Schembri-King, J.; Betageri, R.; Proudfoot, J.R.; Jakes, S. Carboxymethyl-phenylalanine as a replacement for phosphotyrosine in SH2 domain binding. *J. Biol. Chem.* **1998**, *273*, 20238–20242. [[CrossRef](#)]
28. Jorgensen, W.L.; Tirado-Rives, J. The OPLS [optimized potentials for liquid simulations] potential functions for proteins, energy minimizations for crystals of cyclic peptides and crambin. *J. Am. Chem. Soc.* **1988**, *110*, 1657–1666. [[CrossRef](#)]
29. Shivakumar, D.; Williams, J.; Wu, Y.; Damm, W.; Shelley, J.; Sherman, W. Prediction of absolute solvation free energies using molecular dynamics free energy perturbation and the OPLS force field. *J. Chem. Theory Comput.* **2010**, *6*, 1509–1519. [[CrossRef](#)]
30. Jorgensen, W.L.; Maxwell, D.S.; Tirado-Rives, J. Development and testing of the OPLS all-atom force field on conformational energetics and properties of organic liquids. *J. Am. Chem. Soc.* **1996**, *118*, 11225–11236. [[CrossRef](#)]
31. Campagna-Slater, V.; Schapira, M. Evaluation of virtual screening as a tool for chemical genetic applications. *J. Chem. Inf. Model.* **2009**, *49*, 2082–2091. [[CrossRef](#)]
32. Cummings, M.D.; Desjarlais, R.L.; Gibbs, A.C.; Mohan, V.; Jaeger, E.P. Comparison of automated docking programs as virtual screening tools. *J. Med. Chem.* **2005**, *48*, 962–976. [[CrossRef](#)]
33. Harder, E.; Damm, W.; Maple, J.; Wu, C.; Reboul, M.; Xiang, J.Y.; Wang, L.; Lupyan, D.; Dahlgren, M.K.; Knight, J.L.; et al. OPLS3: A force field providing broad coverage of drug-like small molecules and proteins. *J. Chem. Theory Comput.* **2016**, *12*, 281–296. [[CrossRef](#)] [[PubMed](#)]
34. Schrödinger Release 2021-2: *Core Hopping*; Schrödinger, LLC: New York, NY, USA, 2021.

**Disclaimer/Publisher’s Note:** The statements, opinions and data contained in all publications are solely those of the individual author(s) and contributor(s) and not of MDPI and/or the editor(s). MDPI and/or the editor(s) disclaim responsibility for any injury to people or property resulting from any ideas, methods, instructions or products referred to in the content.